

Multimodal Sparse Reconstruction in Lamb Wave Based Structural Health Monitoring

Andrew Golato, Sridhar Santhanam*, Fauzia Ahmad, Moeness G. Amin
Center for Advanced Communications, College of Engineering, Villanova University,
800 E. Lancaster Ave., Villanova, PA 19085, USA.

ABSTRACT

Lamb waves are utilized extensively for structural health monitoring of thin structures, such as plates and shells. Normal practice involves fixing a network of piezoelectric transducers to the structural plate member for generating and receiving Lamb waves. Using the transducers in pitch-catch pairs, the scattered signals from defects in the plate can be recorded. In this paper, we propose an l_1 -norm minimization approach for localizing defects in thin plates, which inverts a multimodal Lamb wave based model through exploitation of the sparseness of the defects. We consider both symmetric and anti-symmetric fundamental propagating Lamb modes. We construct model-based dictionaries for each mode, taking into account the associated dispersion and attenuation through the medium. Reconstruction of the area being interrogated is then performed jointly across the two modes using the group sparsity constraint. Performance validation of the proposed defect localization scheme is provided using simulated data for an aluminum plate.

Keywords: Sparse reconstruction, multimodal, Lamb waves, compressed sensing, structural health monitoring

1. INTRODUCTION

Structural Health Monitoring (SHM) is emerging as a primary technology for the assessment of the integrity of a variety of structures.¹⁻⁴ Much of the recent attention garnered by this field is attributed to the fact that SHM enables self-sensing capabilities in structures. Within the application areas of SHM, the use of guided ultrasonic waves for real-time imaging of defects in thin-walled structures has grown considerably. Such thin-walled structures include airplanes, bridges, and windmills. The addition of a self-sensing system to such structures would carry both safety and economic advantages.⁵

Lamb waves are the preferred wave mode for SHM of thin plate and shell structures due to their ability to travel large distances without significant attenuation, while providing rich interactions with defects.⁶⁻⁸ This preference has only recently emerged, facilitated by advances in computing, processing, and electronics that can handle the complexities of Lamb waves. Lamb waves are the solutions to the wave equation unique to a thin plate with traction free conditions on the plate surfaces.^{9,10} The waves are multimodal and the solutions can be separated into symmetric (S) and anti-symmetric (A) modes. The number of symmetric and anti-symmetric modes present can be regulated by the frequency of the generated signal. While higher frequencies will offer an overabundance of wave modes, only the S_0 and A_0 modes will be present at low frequencies. Additionally, the phase and group velocities of the individual modes are frequency-dependent. As a result, the shape of the waves changes during propagation due to dispersion. Edge reflections and the scatterer-spawning of additional wave modes further complicate the guided Lamb wave signal.^{5,11}

Despite the complexity of the propagating Lamb waves, exploitation of the information contained in the various modes provides an enhanced assessment of the health of the structure. For example, the S_0 mode is appropriate for detecting transverse cracks in the middle of plates, while the S_1 mode is better suited at detecting smaller transverse cracks on the surface of plates. On the other hand, the A_0 and A_1 modes interact with delamination cracks lying in a plane parallel to the plane of the plate.¹²

In order to utilize Lamb waves in SHM, typically, a network of piezoelectric (PZT) transducers is attached to the surface of the structure. Windowed sinusoidal pulses excite a transmitting transducer, which incites elastic stress waves – the Lamb waves – that travel through the thin-walled structure and arrive at the receiving transducers in the network. During their propagation through the structure, the Lamb waves interact with any scatterers present. Once the scattered signal is received, it must be processed in order to extract defect information from it. This processing can take on various forms.

*sridhar.santhanam@villanova.edu; <http://www1.villanova.edu/villanova/engineering/research/centers/cac/facilities/aul.html>

However, most often, it first involves the subtraction of a baseline signal (signal received with no defect present) from the received signal so that the residual displays primarily the effects of the defect.⁵ This is followed by an image formation process to reconstruct the scene, i.e., the area under investigation. Both data-independent and adaptive beamforming approaches have been employed for scene reconstruction in order to detect the presence of defects.^{13,14} However, none of these methods exploit the sparsity of scattering sources or defects in the structure for image recovery. In a very recent work, the defect imaging problem in Lamb wave based SHM was cast in a sparse reconstruction framework by recognizing that the number of defects is typically small.⁵ Reasonably accurate imaging results with sufficient resolution of neighboring defects in the presence of noise were obtained with l_1 -norm minimization approach. However, this work did not take into account the presence of multiple modes.

In this paper, we present a multimodal scene reconstruction approach for localizing defects in thin plates, which inverts a multimodal Lamb wave based model through exploitation of the sparsity of the defects. We consider both symmetric and asymmetric fundamental propagating Lamb modes and construct model-based dictionaries for each mode, taking into account the associated dispersion and attenuation through the medium. Image recovery is then performed jointly across the two modes using the group sparsity constraint.¹⁵⁻¹⁸ The effectiveness of the proposed method is demonstrated using simulated data for an aluminum plate.

The remainder of the paper is organized as follows. In Section 2, we describe the signal propagation model and present the sparse reconstruction algorithm for exploitation of the multiple propagating Lamb modes. Results based on simulated data are discussed in Section 3. Section 4 contains the concluding remarks.

2. MULTIMODAL SIGNAL MODEL AND SPARSE RECONSTRUCTION

2.1 Lamb Wave Propagation and Scattering

Consider a thin plate with a spatially distributed network of J PZT transducers attached to its surface, where each sensor can both transmit and receive signals in the form of Lamb waves. A pitch-catch mode of operation is assumed, i.e., transducers are employed for data collection in pairs with one transducer transmitting the signal and the other acting as the receiver. For J transducers, a total of $L = J(J - 1)/2$ transmit-receive pairs are used.

For the l th transmit-receive pair, let the transmitter and receiver be located at position vectors \mathbf{t}_l and \mathbf{r}_l , respectively. The transmitter is excited by a waveform $h(t)$. Since transmission by PZT transducers is omnidirectional and multimodal, both symmetric and anti-symmetric modes propagate from the transducer, but with different frequency-dependent speeds. Let the center frequency of the transmitted signal be chosen such that the only modes propagating in the plate are the fundamental A_0 and S_0 modes. First, consider propagation between the transmitter and the receiver in the absence of any defects. The A_0 and S_0 components, $G_{l,A_0}^{dir}(\cdot)$ and $G_{l,S_0}^{dir}(\cdot)$, of the direct received signal can be expressed in the frequency domain as

$$G_{l,A_0}^{dir}(f) = (\alpha_l / \|\mathbf{t}_l - \mathbf{r}_l\|_2)^{0.5} H(f) \exp(j 2\pi f \|\mathbf{t}_l - \mathbf{r}_l\|_2 / c_{A_0}(f)), \quad (1)$$

$$G_{l,S_0}^{dir}(f) = (\alpha_l / \|\mathbf{t}_l - \mathbf{r}_l\|_2)^{0.5} H(f) \exp(j 2\pi f \|\mathbf{t}_l - \mathbf{r}_l\|_2 / c_{S_0}(f)), \quad (2)$$

where $H(f)$ is the Fourier transform of $h(t)$, c_{A_0} and c_{S_0} are the frequency-dependent phase speeds of the A_0 and S_0 modes, α_l is a normalizing constant for the distance of the l th transmit-receive pair. The attenuation caused by the geometrical spreading of the circular wavefront is captured by the inverse square root dependence on $\|\mathbf{t}_l - \mathbf{r}_l\|_2$. The time-domain equivalents of the A_0 and S_0 signal components, $g_{l,A_0}^{dir}(t)$ and $g_{l,S_0}^{dir}(t)$, are the inverse Fourier transforms of (1) and (2), respectively. The total received direct signal corresponding to the l th transmit-receive pair is given by

$$z_l^{dir}(t) = g_{l,A_0}^{dir}(t) + g_{l,S_0}^{dir}(t), \quad (3)$$

which serves as the baseline signal for background subtraction. It is noted that additional modes are also generated by signal scatterings from the boundaries of the plate. However, these modes are quite weak provided that the plate boundaries are sufficiently far away from the area being interrogated and are, thus, ignored in this work.

Next, consider a defect located at position vector \mathbf{s}_p . In addition to the direct propagation, both S_0 and A_0 waves will be scattered by the defect towards the receiver at \mathbf{r}_l . The received scattered waves in the frequency domain for the two modes are given by,

$$G_{lp,A_0}^{sc}(f) = \left(\frac{\beta_{lp}}{\|\mathbf{t}_l - \mathbf{s}_p\|_2}\right)^{0.5} \left(\frac{\gamma_{lp}}{\|\mathbf{r}_l - \mathbf{s}_p\|_2}\right)^{0.5} S_{p,A_0}(f, \theta_{l,in}, \theta_{l,out}) H(f) \exp\left(j2\pi f(\|\mathbf{t}_l - \mathbf{s}_p\|_2 + \|\mathbf{r}_l - \mathbf{s}_p\|_2)/c_{A_0}(f)\right), \quad (4)$$

$$G_{lp,S_0}^{sc}(f) = \left(\frac{\beta_{lp}}{\|\mathbf{t}_l - \mathbf{s}_p\|_2}\right)^{0.5} \left(\frac{\gamma_{lp}}{\|\mathbf{r}_l - \mathbf{s}_p\|_2}\right)^{0.5} S_{p,S_0}(f, \theta_{l,in}, \theta_{l,out}) H(f) \exp\left(j2\pi f(\|\mathbf{t}_l - \mathbf{s}_p\|_2 + \|\mathbf{r}_l - \mathbf{s}_p\|_2)/c_{S_0}(f)\right), \quad (5)$$

where β_{lp} and γ_{lp} are the respective normalizing constants for the distances of the l th transmitter and receiver to the p th defect, S_{p,A_0} and S_{p,S_0} are the respective frequency-domain scatterer responses under the A_0 and S_0 modes, which are typically functions of frequency, the incident angle $\theta_{l,in}$ and the scattered angle $\theta_{l,out}$. The equivalent time-domain versions, $g_{lp,A_0}^{sc}(t)$ and $g_{lp,S_0}^{sc}(t)$, are the respective inverse Fourier transforms of eqs. (4) and (5). In the presence of the scatterer at \mathbf{s}_p , the total received signal at \mathbf{r}_l is the sum of the direct and scattered signal components corresponding to the S_0 and A_0 modes,

$$z_l(t) = g_{l,A_0}^{dir}(t) + g_{l,S_0}^{dir}(t) + g_{lp,A_0}^{sc}(t) + g_{lp,S_0}^{sc}(t). \quad (6)$$

For the case of P structural defects in the plate, the total received signal, corresponding to the l th transmit-receive pair, is the superposition of the direct signal and the scattered modes produced by all defects, which can be expressed as

$$z_l(t) = g_{l,A_0}^{dir}(t) + g_{l,S_0}^{dir}(t) + \sum_{p=0}^{P-1} (g_{lp,A_0}^{sc}(t) + g_{lp,S_0}^{sc}(t)). \quad (7)$$

Note that the interactions between the defects are ignored in this model. Background subtraction is applied as follows,

$$\delta z_l = z_l(t) - z_l^{dir}(t) = \sum_{p=0}^{P-1} (g_{lp,A_0}^{sc}(t) + g_{lp,S_0}^{sc}(t)). \quad (8)$$

The l th difference signal, δz_l , contains only the scattered signal components. The direct components are the same over the two measurements and are thus removed from the difference signal.

2.2 Multimodal Linear Signal Model

In this section, we consider the special case of angle- and frequency-independent defect scattering responses. That is, $S_{p,A_0}(f, \theta_{l,in}, \theta_{l,out}) = x_{p,A_0}$ and $S_{p,S_0}(f, \theta_{l,in}, \theta_{l,out}) = x_{p,S_0}$, $\forall f, l$. The more general case of frequency- and angle-dependent scattering responses will be considered in future work.

An equivalent matrix-vector representation of the difference signals, $\delta z_l, l = 0, 1, \dots, L-1$, can be obtained as follows. The area being investigated is conceptualized as a uniform grid of M points representing the potential defect locations, where M is assumed to be much greater than P . That is, most of the area is assumed to be defect-free. Let \mathbf{x}_{A_0} and \mathbf{x}_{S_0} be the concatenated $M \times 1$ scene reflectivity vectors corresponding to the spatial sampling grid under the A_0 and S_0 modes, respectively. Vectors \mathbf{x}_{A_0} and \mathbf{x}_{S_0} can be viewed as the outputs of weighted indicator functions, which take the values x_{p,A_0} and x_{p,S_0} , respectively, if the p th defect exists at the m th grid-point; otherwise, the values are equal to zero. Sampling the l th difference signal δz_l at times $t_k, k = 0, 1, \dots, K-1$, we obtain a $K \times 1$ vector $\Delta \mathbf{z}_l$. Then, using (4), (5), and (8), we obtain the relationship between the l th difference signal and the scene reflectivity vectors as

$$\Delta \mathbf{z}_l = \Psi_{l,A_0} \mathbf{x}_{A_0} + \Psi_{l,S_0} \mathbf{x}_{S_0}, \quad (9)$$

where Ψ_{l,A_0} and Ψ_{l,S_0} are dictionary matrices of dimensions $K \times M$. The m th column of Ψ_{l,A_0} consists of the scattered A_0 wave corresponding to a defect at the m th grid-point \mathbf{s}_m and the k th element of the m th column can be written as

$$[\Psi_{l,A_0}]_{k,m} = \mathcal{F}^{-1} \left\{ \left(\frac{\beta_{lp}}{\|\mathbf{t}_l - \mathbf{s}_m\|_2} \right)^{0.5} \left(\frac{\gamma_{lp}}{\|\mathbf{r}_l - \mathbf{s}_m\|_2} \right)^{0.5} H(f) \exp\left(j2\pi f(\|\mathbf{t}_l - \mathbf{s}_m\|_2 + \|\mathbf{r}_l - \mathbf{s}_m\|_2)/c_{A_0}(f)\right) \right\} \Big|_{t=t_k}. \quad (10)$$

Likewise, the m th column of Ψ_{l,S_0} consists of the scattered S_0 wave corresponding to a defect at \mathbf{s}_m with its k th element given by

$$[\Psi_{l,S_0}]_{k,m} = \mathcal{F}^{-1} \left\{ \left(\frac{\beta_{lp}}{\|\mathbf{t}_l - \mathbf{s}_m\|_2} \right)^{0.5} \left(\frac{\gamma_{lp}}{\|\mathbf{r}_l - \mathbf{s}_m\|_2} \right)^{0.5} H(f) \exp\left(j2\pi f(\|\mathbf{t}_l - \mathbf{s}_m\|_2 + \|\mathbf{r}_l - \mathbf{s}_m\|_2)/c_{S_0}(f)\right) \right\} \Big|_{t=t_k}. \quad (11)$$

Eq. (9) considers the contribution of only one transmit-receive pair. Stacking the difference signal vectors corresponding to all L pairs forms the $KL \times 1$ vector

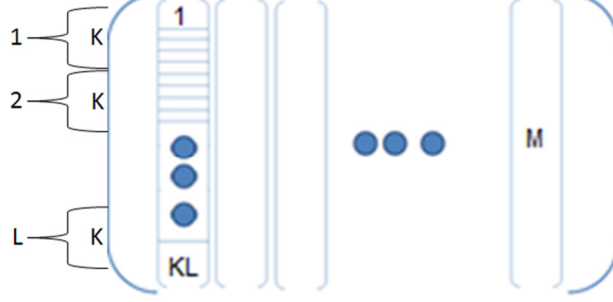


Figure 1. Structure of the dictionary corresponding to a single mode. Each column corresponds to a particular grid-point and consists of L blocks. Each block corresponds to a unique transmit-receive pair and consists of K elements resulting from K time samples per pairing.

$$\Delta \mathbf{z} = [\Delta \mathbf{z}_0^T \quad \Delta \mathbf{z}_1^T \quad \cdots \quad \Delta \mathbf{z}_{L-1}^T]^T, \quad (12)$$

where the superscript ‘ T ’ denotes the matrix transpose operation. Eqs. (9) and (12) together yield the linear system of equations

$$\Delta \mathbf{z} = \Psi_{A_0} \mathbf{x}_{A_0} + \Psi_{S_0} \mathbf{x}_{S_0}, \quad (13)$$

where

$$\Psi_{A_0} = [\Psi_{0,A_0}^T \quad \Psi_{1,A_0}^T \quad \cdots \quad \Psi_{L-1,A_0}^T]^T, \quad \Psi_{S_0} = [\Psi_{0,S_0}^T \quad \Psi_{1,S_0}^T \quad \cdots \quad \Psi_{L-1,S_0}^T]^T \quad (14)$$

denote the respective dictionaries of size $KL \times M$ corresponding to the A_0 and S_0 propagation modes. The structure of each dictionary is illustrated in Fig. 1.

2.3 Group Sparse Reconstruction

The reflectivity of the defects usually tends to vary under the two fundamental modes. In general, no prior knowledge of the exact relationship between \mathbf{x}_{A_0} and \mathbf{x}_{S_0} can be assumed. However, since both reflectivity vectors represent the same scene, they share a common support. That is, if a particular element of \mathbf{x}_{A_0} is nonzero, then so should be the corresponding element of \mathbf{x}_{S_0} . This calls for a group sparse reconstruction, which is described below.

First, the vectors \mathbf{x}_{A_0} and \mathbf{x}_{S_0} are stacked to form a single tall vector $\mathbf{x} = [\mathbf{x}_{A_0}^T \quad \mathbf{x}_{S_0}^T]^T$. Then, $\Delta \mathbf{z}$ can be expressed as

$$\Delta \mathbf{z} = \Psi \mathbf{x}, \quad (15)$$

where $\Psi = [\Psi_{A_0} \quad \Psi_{S_0}]$. The nonzero values in \mathbf{x} appear in groups of length two rather than being arbitrarily spread throughout the vector. The group-sparse vector \mathbf{x} can be recovered from the measurements $\Delta \mathbf{z}$ in (15) through a mixed l_2/l_1 norm optimization¹⁵ or a block version of the Orthogonal Matching Pursuit algorithm (BOMP)¹⁶. In this work, we employ the latter for scene recovery.

In order to exploit the power received through multimodal propagation, the recovered vectors $\hat{\mathbf{x}}_{A_0}$ and $\hat{\mathbf{x}}_{S_0}$ have to be combined to obtain a single composite scene representation $\tilde{\mathbf{x}}$. We achieve this by calculating the l_2 norm across the elements of these vectors as¹⁷

$$[\tilde{\mathbf{x}}]_m = \tilde{x}_m = \left\| [\hat{x}_{m,A_0} \quad \hat{x}_{m,S_0}]^T \right\|_2. \quad (16)$$

3. SIMULATION RESULTS

We consider a network of 4 transducers (A, B, C, and D) located in the corners of a 2 ft \times 2 ft square region, which is centered on the surface of a 4 ft \times 4 ft aluminum plate of thickness 3 mm, as shown in Fig. 2. There are a total of $L = 6$

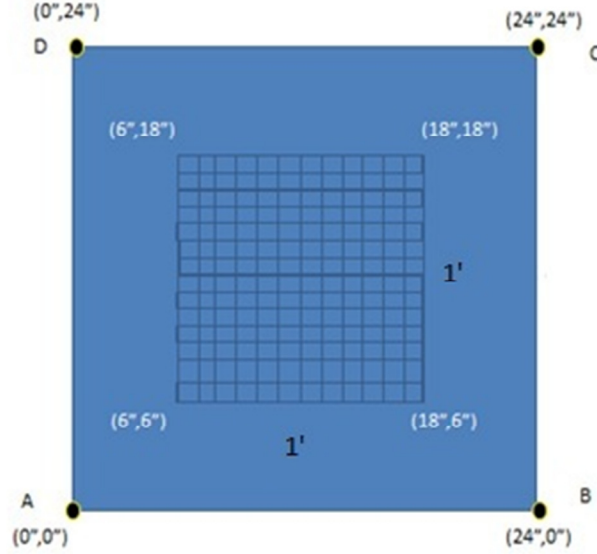


Figure 2. Schematic of the simulation setup. Only the part of the plate containing the transducers and the defects is shown.

distinct transmit-receive pairs, which are used in a sequential manner. The excitation is chosen to be a Hanning-windowed, five-cycle burst of a 100 kHz sinusoidal signal. The corresponding velocities, c_{A_0} and c_{S_0} , for the A_0 and S_0 modes at 100 kHz are 2700 m/s and 5400 m/s, respectively. However, the phase speeds vary with frequency and this dependency is built into the dictionary matrices. The origin of the coordinate system is positioned at the lower left transducer, labeled as “A” in Fig. 2. The region under investigation is selected as a 1 ft \times 1 ft square, centered at (1, 1) ft and divided into 49×49 ($M = 2401$) grid points. Two defects, modeled as point scatterers, are located at (0.8, 0.9) ft and (1.1, 1.2) ft, respectively. The former is assumed to produce a strong scattered S_0 mode ($x_{0,S_0} = 1$) but a weak A_0 mode ($x_{0,A_0} = 0.1$), whereas the latter produces a strong A_0 mode ($x_{1,A_0} = 1$) and a weak S_0 mode ($x_{1,S_0} = 0.1$). The scattered signal corresponding to each transmit-receive pair is sampled at 1 MHz and consists of $K = 600$ time samples. White noise with 0 dB signal-to-noise ratio (SNR) is added to the simulated measurements. Thus, the concatenated received signal, $\Delta \mathbf{z}$, corresponding to all 6 transmit-receive pairs comprises 3600 time samples. Various components of the noise-free concatenated scattered signals are depicted in Fig. 3. We observe that the modal contributions are separable in this case while the contribution from each defect for a given wave mode is unresolvable. However, this will not always be the case as it depends on the number and locations of defects, the choice of the operational frequency, and the transducer network configuration. The dictionaries, Ψ_{A_0} and Ψ_{S_0} , corresponding to the individual A_0 and S_0 modes, are of size 3600×2401 each, whereas the multimodal dictionary Ψ of (15) has the dimensions 3600×4802 .

We first use single-mode based sparse scene recovery by employing Ψ_{S_0} and Ψ_{A_0} independently. That is, we use orthogonal matching pursuit¹⁹ (OMP) to reconstruct the sparse vector $\mathbf{x}_{A_0}(\mathbf{x}_{S_0})$ by only considering the linear signal model $\Delta \mathbf{z} = \Psi_{A_0} \mathbf{x}_{A_0}$ ($\Delta \mathbf{z} = \Psi_{S_0} \mathbf{x}_{S_0}$). The number of OMP iterations was set to 2. Figs. 4(a) and (b) depict the single-mode sparse reconstruction results for the A_0 and S_0 modes, respectively, each of which is averaged over 100 Monte Carlo runs. With one defect preferentially reflecting A_0 mode and the other defect favoring the S_0 mode, each single mode reconstruction is able to identify only one of the two targets. The location of the second grid-point, populated by OMP, is distributed throughout the scene across the various Monte Carlo runs and, as such, is not visible within the dynamic range of the averaged results in Figs. 4(a) and (b). We next use BOMP with 2 iterations to perform the proposed group sparse multi-modal reconstruction. The corresponding result, averaged over 100 Monte Carlo runs, is shown in Fig. 4(c), which clearly provides superior performance by correctly detecting and locating both defects.

This example highlights the shortcoming of single-mode based sparse reconstruction. Since different defects may favor one fundamental mode over another⁸, reconstruction based only on A_0 mode may fail to detect and localize all defects. In the absence of any prior knowledge of the type of defect that may be present in the structure under examination, the only way to ensure an accurate and robust reconstruction is to utilize the multimodal approach.

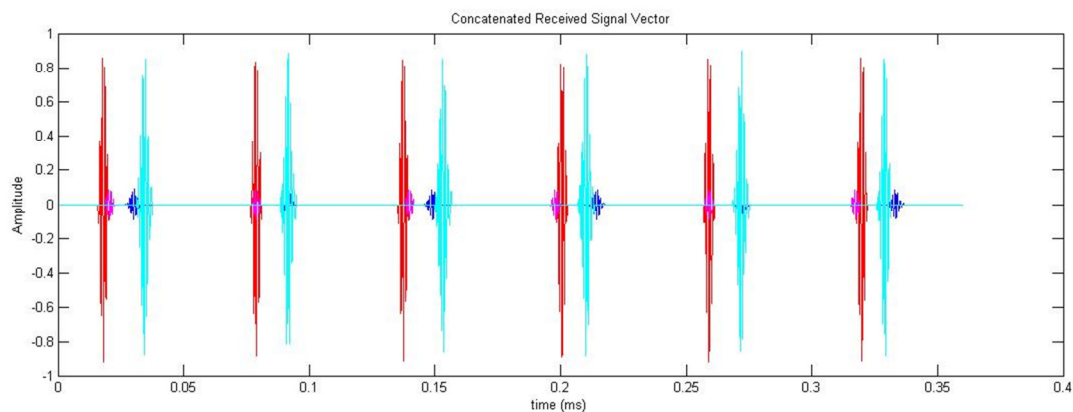


Figure 3. Various components of the concatenated received signal: Scattered S_0 modes from the first (red) and second (magenta) targets, and the scattered A_0 modes from the first (blue) and second (cyan) targets.

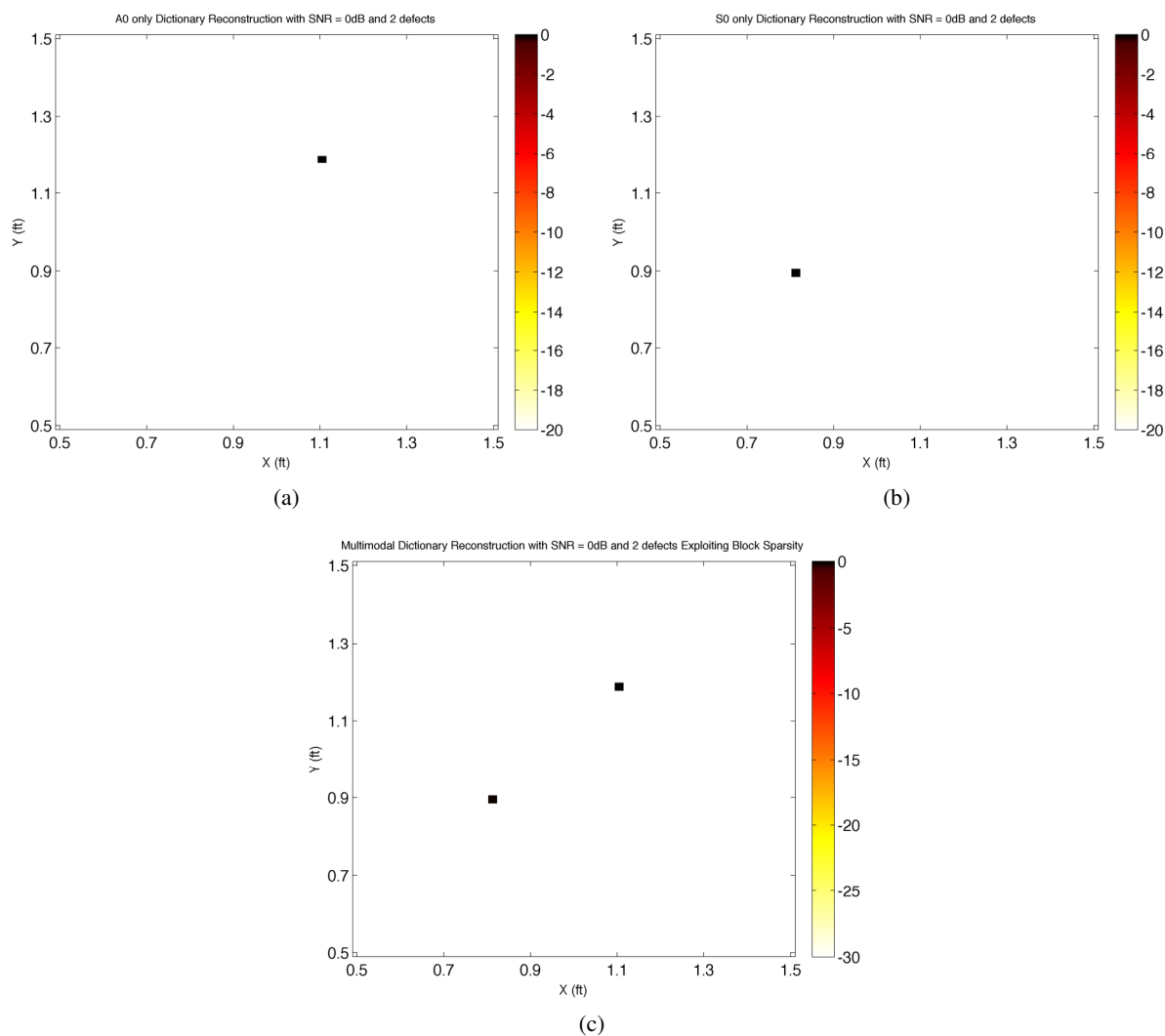


Figure 4. Sparse reconstruction results using the (a) A_0 mode dictionary only, (b) the S_0 mode dictionary only, and (c) group sparse approach based on the multimodal dictionary.

4. CONCLUSION

We have proposed a sparse reconstruction approach, which exploits both symmetric and anti-symmetric fundamental Lamb modes for localizing defects in thin plates. We constructed model-based dictionaries for each mode, taking into account the associated dispersion and attenuation through the medium, followed by sparse reconstruction of the area being interrogated jointly across the two modes using the notion of group sparsity. Superior performance of the multimodal approach relative to single-mode sparse reconstruction was demonstrated using simulation results. We are currently working on experimental validation of the proposed multimodal approach.

ACKNOWLEDGMENT

This research is supported in part by the National Science Foundation (NSF) under grant number IIP-0917690.

REFERENCES

- [1] Kessler, S. S., Spearing, S. M. and Soutis, C., "Structural health monitoring in composite materials using Lamb wave methods," *Smart Materials and Structures* 11(2), 269-278 (2002).
- [2] Raghavan, A. and Cesnik, C. E. S., "A review of guided wave structural health monitoring," *Shock and Vibrations Digest* 39(2), 91-114 (2007).
- [3] Giurgiutiu, V. and Santoni-Bottai, G., "Structural health monitoring of composite structures with piezoelectric wafer active sensors," *AIAA Journal* 49(3), 565-581 (2011).
- [4] Santhanam, S. and Demirli, R., "Reflection and transmission of fundamental Lamb wave modes obliquely incident on a crack in a plate," *Proc. IEEE Int. Ultrasonics Symp.*, 2690-2693 (2012).
- [5] Levine, R. M. and Michaels, R. M., "Model-based imaging of damage with Lamb waves via sparse reconstruction," *J. Acoust. Soc. Am.* 133(3), 1525-1534 (2013).
- [6] Ramadas, C., Balasubramaniam, K., Joshi, M., and Krishnamurthy, C., "Interaction of the primary antisymmetric Lamb mode with the symmetric delaminations: numerical and experimental studies," *Smart Mater. Struct.* 18(1), 1-7 (2009).
- [7] Sohn, H., Park, G., Walt, J., Limback, N. P. and Farrar, C., "Wavelet based active sensing for delamination detection in composite structures," *Smart Mater. Struct.* 13(1), 153-160 (2004).
- [8] Tua, P., Quek, S. and Wang, Q., "Detection of cracks in plates using piezo-actuated Lamb waves," *Smart Mater. Struct.* 13(1), 643-660 (2004).
- [9] Achenbach, J., [Wave Propagation in Elastic Solids], North Holland, New York (1984).
- [10] Rose, J., [Ultrasonic Waves in Solid Media], Cambridge University Press, Cambridge, UK (1999).
- [11] Santhanam, S. and Demirli, R., "Reflection of Lamb waves obliquely incident on the free edge of a plate," *Ultrasonics* 53(1), 271-282 (2013).
- [12] Ng, C. and Veidt, M., "Scattering of the fundamental antisymmetric Lamb wave at delaminations in composite laminates," *J. Acoust. Soc. Am.* 129(1), 1288-1296 (2011).
- [13] Johnson, D. H. and Dudgeon, D. E., [Array Signal Processing: Concepts and Techniques], Prentice Hall, (1993).
- [14] Hall, J. and Michaels, J., "Minimum variance ultrasonic imaging applied to an in situ sparse guided wave array," *IEEE Trans. Ultrason., Ferroelectr., Freq. Control* 57 (10), 2311-2323 (2010).
- [15] Yuan, M. and Lin, Y., "Model selection and estimation in regression with grouped variables," *J. Royal Stat. Soc. Series B* 68(1), 49-67 (2007).
- [16] Eldar, Y. C., Kuppinger, P. and Bolcskei, H., "Block-sparse signals: Uncertainty relations and efficient recovery," *IEEE Trans. Signal Process.* 58(6), 3042-3054 (2010).
- [17] Leigsnering, M., Ahmad, F., Amin, M. and Zoubir, A., "Compressive sensing based specular multipath exploitation for through-the-wall radar imaging," *Proc. IEEE Int. Conf. Acoust., Speech, Signal Process.*, 6004-6008 (2013).
- [18] Amin, M. G. and Ahmad, F., "Compressive sensing for through-the-wall radar imaging," *J. Electron. Imaging*. 22(3), 030901 (2013).
- [19] Tropp, J.A., "Greed is good: algorithmic results for sparse approximation," *IEEE Trans. Inf. Theory*. 50(10), 2231-2242 (2004).